Available online at www.sciencedirect.com

ScienceDirect

Nuclear and Particle Physics Proceedings 273–275 (2016) 1513–1518

www.elsevier.com/locate/nppp

The onset on the ridge structure in AA, pA and pp collisions

C. Andrés[a], A. Moscoso[a], C. Pajares[a,*]

[a]*Departamento de Física de Partículas and IGFAE, Universidade de Santiago de Compostela, 15782, Santiago de Compostela, Spain*

Abstract

It is shown that the anomalous sharp increasing of the strength of the near-side ridge structures observed in Au-Au collisions at $\sqrt{s}$ = 62 GeV and $\sqrt{s}$ = 200 GeV and the onset of the ridge structure in pPb and in pp collisions can be naturally explained in the framework of string percolation. In all the cases the near-side strength reflects the collision area covered by the strings stretched between the colliding objects and therefore it is related to the shape of their profile functions. The dependence of the pseudorapidty and azimuthal widths on multiplicty and energy is qualitatively explained.

Keywords: ridge structure, string percolation

1. Introduction

Correlations between pairs of hadrons that are collimated in their relative azimuthal angle and are long range in relative rapidity were observed in heavy ion collisions at RHIC energies [1, 2, 3, 4, 5, 6] and later at LHC energies [7]. These ridge-like correlations have also been seen in proton-proton collisions at $\sqrt{s}$ = 7 TeV for high multiplicity events [8]. More recently, a sizable ridge has been seen in p-Pb collisions at $\sqrt{s}$ = 5.02 TeV [9, 10, 11, 12, 13]. Much attention has been paid to understand whether these structures are due to initial state or to final state effects that are amenable to a hydrodynamic description [14, 15, 16, 17, 18, 19, 20, 21, 22, 23, 24, 25, 26, 27].

The origin of long range rapidity correlations is similar in heavy ion and proton-proton collisions and it is explained, in the glasma picture of the Color Glass Condensate (CGC), due to the saturation of color flux tubes correlated in the transverse space with a length $1/Q_s$ determined by the saturation momentum Q_s [18, 19, 20, 21, 22, 23, 24]. On the contrary, not much attention has been paid to the onset of the ridge structure. In pp collisions at $\sqrt{s}$ = 7 TeV the structure is only observed for $N_{ch} > 110$ and in pPb collisions at $\sqrt{s}$ = 5.02 TeV for $N_{ch} \gtrsim 50$. Moreover, in Au-Au collisions at $\sqrt{s}$ = 200 GeV and $\sqrt{s}$ = 62 GeV an anomalous centrality dependence of the correlation is observed: the strength of the near-side ridge as a function of multiplicity presents a change on the behavior of the slope for N_{ch} = 120 and N_{ch} = 130 respectively [28].

In this paper, we show that all these features can be understood in the framework of percolation of strings. As the number of strings formed in a collision reaches an universal critical density, a macroscopic cluster of strings appears covering around 2/3 of the total collision area [29]. As the density approaches the critical value the ridge structure begins to unfold. The dependence of the strength of the near-side ridge on the multiplicity in a given collision reflects the fraction of the collision area covered by strings which is related to the profile function of the colliding objects.

2. The near-side ridge in the string percolation model

In the string percolation model, multiparticle production is described in terms of color strings stretched

*Corresponding author

Email addresses: carlota.andres@usc.es (C. Andrés), alexis.moscoso@rai.usc.es (A. Moscoso), pajares@fpaxp1.usc.es (C. Pajares)

http://dx.doi.org/10.1016/j.nuclphysbps.2015.09.245

among the partons of the projectile and the target. These strings decay into new ones by $q-\bar{q}$ and $qq-\bar{q}\bar{q}$ pair production and subsequently hadronize producing the observed hadrons. Due to confinement, the color of these strings is confined to a small area in the transverse space, $S_1 = \pi r_0^2$, with $r_0 \simeq 0.2$ fm. With increasing energy and/or atomic number of the colliding particles, the number of strings grows and they start to overlap forming clusters, very similar to discs in two-dimensional percolation theory. Defining the density of strings as $\rho = N_s \frac{S_1}{S_A}$, where S_A is the collision area and N_s the number of strings, at a critical density ρ_c = 1.2-1.5 a macroscopical cluster appears, which marks the percolation phase transition. The value of ρ_c varies between 1.2 and 1.5 depending on the profile used (1.2 in the homogeneous case and 1.5 for the Gaussian or Wood-Saxon type) [30].

A cluster of n strings behaves as a single string with energy-momentum corresponding to the sum of the individual ones and with a higher color field corresponding to the vectorial sum in color space of the color fields of the individual strings. Due to the randomness of the color field, the strength of the resulting color field is not n times the strength of the individual color field but $\sqrt{n}$. Due to this fact, the multiplicity and transverse momentum of the clusters are given by [31, 32]:

$$\mu_n = \sqrt{n\frac{S_n}{S_1}}\mu_1, \quad \langle p_T^2\rangle_n = \sqrt{n\frac{S_1}{S_n}}\langle p_T^2\rangle_1, \tag{1}$$

where μ_1 and $\langle p_T^2\rangle_1$ are, respectively, the multiplicity and the p_T^2 of the particles produced by a single string and S_n is the area covered by n strings. In the high density limit the formula (1) can be written as [31]:

$$\mu_n = N_s F(\rho)\mu_1, \quad \langle p_T^2\rangle_n = \langle p_T^2\rangle_1 / F(\rho), \tag{2}$$

where

$$F(\rho) = \sqrt{\frac{1-e^{-\rho}}{\rho}}. \tag{3}$$

Assuming a homogeneus profile for the collision area, the distribution of the overlapping of n strings is Poissonian with a mean value ρ, $P_n = \frac{\rho^n}{n!}e^{-\rho}$. Hence, in (3), $1-e^{\rho}$ is the fraction of the area covered by strings. A more realistic profile implies a modification of the area covered by strings in formula (3).

The area covered by clusters divided by the area of an effective cluster gives the effective average number $\langle N\rangle$ of clusters

$$\langle N\rangle = \frac{(1-e^{-\rho})R^2}{r_0^2 F(\rho)} = \sqrt{1-e^{-\rho}}\,\sqrt{\rho}\left(\frac{R}{r_0}\right)^2. \tag{4}$$

Each one of these clusters $\langle N\rangle$ contains $N_s/\langle N\rangle = 1/F(\rho)$ strings. Therefore, these effective clusters have a rapidity length

$$\sigma y_N = \Delta y_1 - \ln F(\rho) = \Delta y_1 + \ln\sqrt{\frac{\rho}{1-e^{-\rho}}}, \tag{5}$$

where Δy_1 is the rapidity length of one string. In most strings models [33, 34, 35, 36, 37], the main contribution to the multiplicity comes from strings stretched between sea quarks and antiquarks being proportional to the difference between the number of collisions and the number of participants. Consequently, summing the energy of these strings, we have as a good approximation for Δy_1

$$\Delta y_1 = c\left(1-\frac{N_A}{N_C}\right)\ln\left(\frac{s}{s_0}\right). \tag{6}$$

The normalized two-particle correlation function can be written in the two step scenario [31, 32] as the normalized fluctuation in the number of effective strings

$$\mathcal{R} \equiv \frac{\langle n^2\rangle - \langle n\rangle^2 - \langle n\rangle}{\langle n\rangle^2} = \frac{\langle N^2\rangle - \langle N\rangle^2}{\langle N^2\rangle} = \frac{1}{k}, \tag{7}$$

where n is the multiplicity of the produced particles. If the particle distribution is a negative binomial, as in the case of string percolation, with parameter K_{NB} then $k = K_{NB}$. In the low density regime, ρ small, the multiplicity distribution is essentially Poisson-like and therefore $k \to \infty$. In the large density limit, assuming that the N effective clusters behave like a single one, $\langle N^2\rangle - \langle N\rangle^2 \approx \langle N\rangle$, then $k \to \langle N\rangle \to \infty$ [32, 38]. At intermediate string density, k must have a minimum close to the critical string density. A parametrization of k satisfying the above requirements is [26]

$$k = \frac{\sqrt{\rho}\,(R/r_0)^2}{1-e^{-\rho}} = \frac{\langle N\rangle}{(1-e^{-\rho})^{3/2}}. \tag{8}$$

The two particle correlations can be written as [18]

$$\frac{\Delta\rho}{\sqrt{\rho_{ref}}} = \mathcal{R}\frac{dn}{dy}G(\phi), \tag{9}$$

where G(ϕ) describes the azimuthal dependence. The centrality dependence is encoded in $\mathcal{R}\frac{dn}{dy}$. As usual, in equation (9), $\Delta\rho$ is the difference between the pair distribution and the uncorralated pair distribution ρ_{ref} obtained from mixed events.

From equations (4), (6), (7) and (8) we deduce that the strength of the near-side ridge structure, A_1, is proportional to

$$\mathcal{R}\frac{dn}{dy} = \frac{\langle N\rangle}{k} = (1-e^{-\rho})^{3/2}. \tag{10}$$

From equations (5) and (6), the width of the pseudo-rapidity near-side ridge is given by

$$\sigma_{\Delta y} = c\left(1 - \frac{N_A}{N_C}\right)\ln\frac{s}{s_0} + \ln\sqrt{\frac{\rho}{1-e^{-\rho}}}. \qquad (11)$$

As previously mentioned, the factor $1 - e^{-\rho}$ representing the fraction of the collision surface covered by strings was obtained in the high density limit and assuming a homogeneous profile [31]. For more realistic profiles, this shape is modified. For Gaussian and Wood-Saxon profiles, the critical percolation density is not 1.2 but 1.5 and the fraction of the collision area covered by strings is more similar to [30]

$$A(\rho) = \frac{1}{1 + ae^{-(\rho-\rho_c)/b}}, \qquad (12)$$

where ρ_c =1.5. The parameter b controls the ratio between the edge (2πR) over the total surface (πR^2) and therefore is proportional to the inverse of the radius.

3. Comparison with experimental data (RHIC, LHC)

In order to compare with the experimental data on the strength of the near-side ridge we use equation (12), fitting the expression $A_1 = cA(\rho)^{1/3}$ to the data on Au-Au collisions at $\sqrt{s}$ = 200 GeV and $\sqrt{s}$ = 62 GeV and pPb and pp collisions at $\sqrt{s}$ = 5.02 TeV and $\sqrt{s}$ = 7 TeV respectively. To do this we need to know the values of ρ. They are taken from a previous study in the framework of string percolation of dN/dy at SPS, RHIC and LHC energies for pp and AA at different centralities [39, 40]. In the case of pp and pPb to compute ρ we use the collision area of references [24] and [25]. The values of ρ for Au-Au collisions at $\sqrt{s}$ = 200 GeV for the different centralities are in the range 0.6-3.0. For pPb at $\sqrt{s}$ = 5.02 TeV the values of ρ are between 0.8-2.3 corresponding to N_{ch} = 50 and to N_{ch} = 330, respectively, and for pp at $\sqrt{s}$ = 7 TeV the values are in the range 0.25-0.7, corresponding to N_{ch} = 18 (minumum bias) and N_{ch} = 110, respectively. In high multiplicity pp collisions at LHC the values of ρ are close to the values obtained in peripheral Cu-Cu collisions at RHIC energies, where a ridge structure was observed. This fact, was the main reason to predict [16] the near-side ridge later observed. An example of the dependence of ρ on centrality is shown in Fig. 1 for Au-Au collisions at $\sqrt{s}$ = 200 GeV.

In Fig. 2 we show our results on the strength, A_1, of the near-side ridge as a function of the charged particles for Au-Au collisions at $\sqrt{s}$ = 200 GeV and $\sqrt{s}$ = 62 GeV. The values of the parameters obtained are a = 1.5

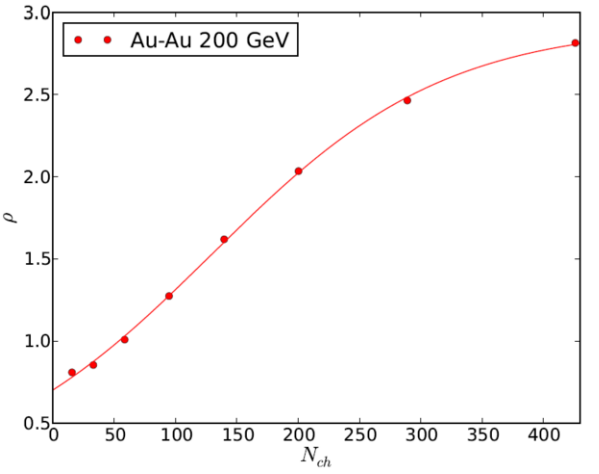

Figure 1: (Color online.) String density ρ plotted as a function of N_{ch} for Au-Au collisions at $\sqrt{s}$ = 200 GeV.

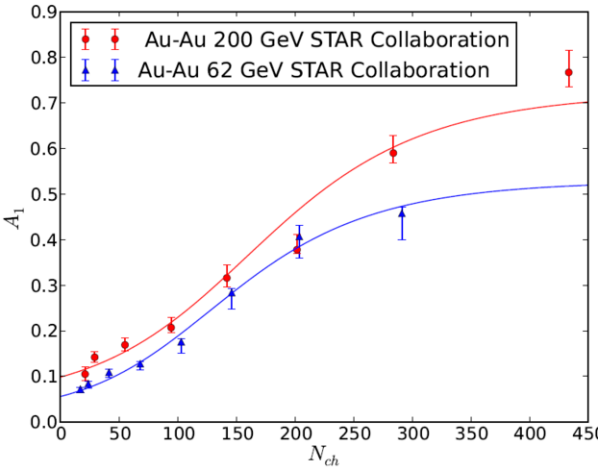

Figure 2: (Color online.) Comparison between our results on the strength of the near-side ridge for Au-Au collisions at two RHIC energies $\sqrt{s}$ = 200 GeV (red line) and $\sqrt{s}$ = 62 GeV (blue line) with experimental data [28] in terms of N_{ch}.

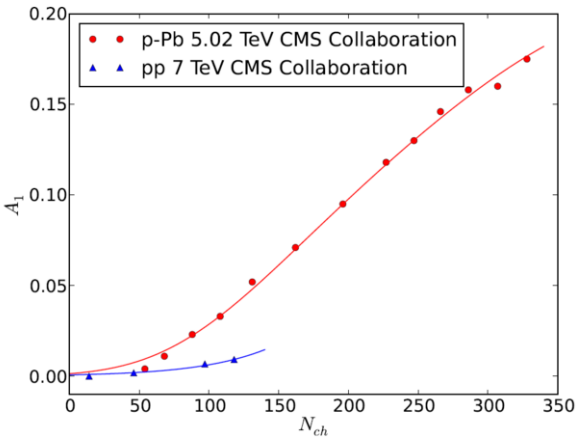

Figure 3: (Color online.) Comparison between our results on the strength of the near-side ridge for pp collisions at $\sqrt{s}$ = 7 TeV (blue line) and pPb collisions $\sqrt{s}$ = 5.02 TeV (red line) with experimantal data [9] versus N_{ch}.

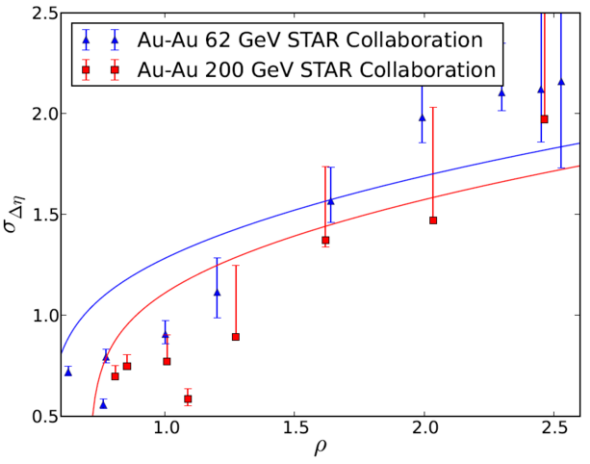

Figure 4: (Color online.) Pseudorapidity width of the near-side ridge for Au-Au collisions at two RHIC energies $\sqrt{s}$ = 200 GeV and $\sqrt{s}$ = 62 GeV [28] plotted as a function of ρ. Curves obtained from equation (11) for Au-Au collisions at $\sqrt{s}$ = 200 GeV (red) and $\sqrt{s}$ = 62 GeV (blue).

and $b = 0.75$. In Fig. 3 we show our results for pPb and pp. In this case, the parameters are $a = 1.5$ and $b = 0.35$. We obseve that the value of b in the pPb and pp case is much smaller than in the case of Au-Au collisions as it was expected. Notice that the string density in pPb at $N_{ch} = 50$, where the near-side ridge structure emerges, is $\rho = 0.8$. In the pp case the near-side ridge structure unfolds at $N_{ch} = 100$, corresponding to $\rho = 0.7$, very close to the obtained one for pPb collisions. Notice that, apart from the normalization constant c, different for the three type of collisions, we fix the parameters $\rho_c = 1.5$ and $a = 1.5$ for all the considered collisions, keeping b as the only fitting parameter. However, this parameter is not fully free because its dependence on the nucleus radius should be similar to $1/R$.

In Fig. 4 we compare our results on the pseudorapidity width, obtained from equation (11) with the experimental results on Au-Au at $\sqrt{s}$ = 200 GeV and $\sqrt{s}$ = 62 GeV [28]. The value of c is 0.23. N_A and N_C are taken from the quoted experimental analysis [41]. It is observed that our result for $\sqrt{s}$ = 200 GeV is slightly larger than the corresponding one at $\sqrt{s}$ = 62 GeV. Experimental data are very close at both energies.

The main aim of this paper is not a detailed description of the azimuthal dependence of the near-side ridge. However, a brief discussion on this in the framework of percolation of strings is in order. The conventional understanding of the ridge is simply related to flow harmonics in a fluid dynamic scenario, where the inclusion of the pp ridge is a challenge. In string percolation, the initial spatial anisotropy is translated into transverse momentum anisotropy assuming that in the transverse momentum distribution an azimuthal string density, ρ_φ, instead of the string density ρ, is introduced:

$$\rho_\varphi = \rho \left(\frac{R}{R_\varphi}\right)^2, \tag{13}$$

where

$$R_\varphi = \frac{\sin(\varphi - \alpha)}{\sin\varphi}, \quad \sin\alpha = \frac{b\sin\varphi}{2R_A}, \tag{14}$$

being b the impact parameter of the collision. R is given by

$$\frac{\pi R^2}{4} = \frac{1}{2}\int_0^{\frac{\pi}{2}} R_\varphi^2 d\varphi \quad \text{or} \quad R^2 = \langle R_\varphi^2 \rangle \tag{15}$$

as it can be seen in Fig. 5.

Using equation (13) an analytical expression for the elliptic flow v_2 which properly describes the RHIC and LHC data for π, k and p and the centrality, energy, rapidity and transverse momentum without hydordynamical evolution is obtained [42, 43, 44].

There are two arguments in support of equation (13). One single string in the transverse plane is seen as a circle filled with colour field. The breaking of the string produces partons, which eventually hadronize, being emitted from the surface of the circle. Therefore, no anisotropy is expected. Nevertheless, the shape of a cluster formed by several overlapping strings is not a

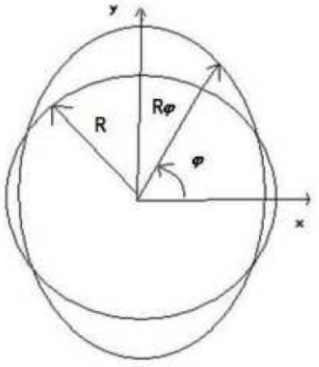

Figure 5: Scheme of the reaction plane

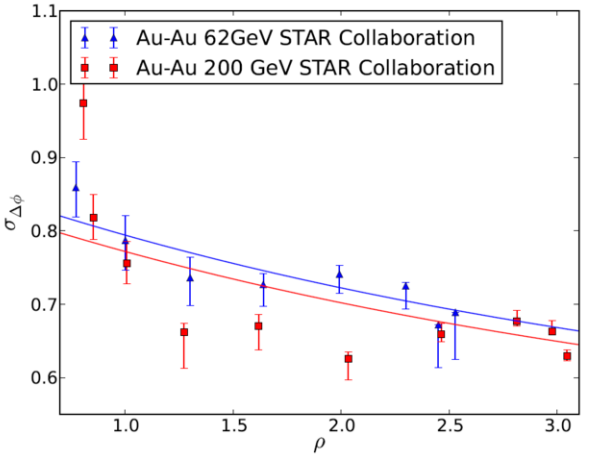

Figure 6: (Color online.) Azimuthal width of the near-side ridge for Au-Au collisions at $\sqrt{s}$ = 200 GeV and $\sqrt{s}$ = 62 GeV [28] versus ρ. Curves obtained from equation (16) for Au-Au collisions at $\sqrt{s}$ = 200 GeV (red) and $\sqrt{s}$ = 62 GeV (blue).

circle and consequently anisotropy is produced. This kind of elliptic flow can be seen as an initial state effect, being similar to the anistropy produced by colour field domains proposed in [27].

There is another argument in favour of equation (13). In the fragmentation of a cluster of strings, the produce partons lose energy due to the interaction with the colour field of othe clusters. This lost energy has been computed [45] leading to similar results to the obtained ones using equation (13). In this case, an agreement with the trend of the data for for different harmonics is also obtained [46]. Now, elliptic flow is seen as a final state effect amenable to a hydrodynamic description.

The narrow structure in the azimuthal dependence of the near-side ridge is determined by the transverse momentum correlation length, which according to equation (2) is $r_0 F(\rho)^{1/2}$. Hence, the width of the azimuthal angle is:

$$\sigma_{\Delta\phi} = c_2 \left(\frac{1 - e^{-\rho}}{\rho} \right)^{1/4} . \qquad (16)$$

In the color glass condensate approach, the origin of the narrow width in azimuth is also the transverse momentum length, given by $1/Q_s$. In the high density limit, Q_s behaves like $\rho^{1/2}$ and consequently $\sigma_{\Delta\phi}$ has the same dependence on centrality and on energy in both approaches. We can translate the equation (13) into terms of the gluon saturation momentum,

$$Q^2_{s\varphi} = Q^2_s \frac{R}{R_\varphi} \qquad (17)$$

and directly obtain the elliptic flow.

In Fig. 6 experimental data on the azimuthal width for Au-Au collisions at $\sqrt{s}$ = 200 GeV and $\sqrt{s}$ = 62 GeV [28] are compared to our model. The values of c_2 are c_2 = 0.866 for Au-Au at $\sqrt{s}$ = 200 GeV and c_2 = 0.890 for Au-Au at $\sqrt{s}$ = 62 GeV. The azimuthal width decreases with increasing energy and centrality in agreement with the trend of the experimental data. For both widths a qualitative agreement is obtained.

The dependence of A_1, $\sigma_{\Delta\eta}$ and $\sigma_{\Delta\phi}$ on energy and centrality, resulting from equations (10) and (12), is very similar to the obtained one in the glasma picture. In this approach, $\mathcal{R}dN/dy$ and $\sigma_{\Delta\eta}$ are proportional to $1/\alpha_s(Q_s)$ and $\sigma_{\Delta\phi}$ is proportional to $1/Q_s$. Hence, both $\mathcal{R}dN/dy$ and $\sigma_{\Delta\eta}$ grow with $\log s$ and $\log N_A$. In the high density limit, we obtain in percolation the same dependence on s and on N_A for both observables. In the case of $\sigma_{\Delta\phi}$, as $1/Q_s \sim N_A^{1/6} s^{\Delta/2}$ and $r_0 F(\rho)^{1/2} \sim r_0 \rho^{1/4} \sim r_0 N_A^{1/6} s^{\Delta/2}$.

4. Conclusions

In conclusion, we have shown that percolation of strings naturally explains the anomalous dependence of the near-side ridge structure correlation on the multiplicity observed in Au-Au collisions at $\sqrt{s}$ = 200 GeV and $\sqrt{s}$ = 62 GeV. The onset of the ridge structure in high multiplicity pp events at $\sqrt{s}$ = 7 TeV and in high multiplicity pPb at $\sqrt{s}$ = 5.02 TeV are also explained. Furthermore, our model qualitatively describes the dependence of the azimuthal and pseudorapidity widths on multiplicity. Our framework can be regarded as a complementary picture to the glasma in the description of

the initial state, able to explore the transition from low to high density.

Acknowledgements

We thank G. Feofilov, M. A. Braun, N. Armesto and C. Salgado for very useful discussions. This work has been done under the project FPA2011-22776 of MINECO (Spain), the Spanish Consolider CPAN project, FEDER funds and Xunta de Galicia (GRC 2013-024).

References

[1] J. Adams. *et al.* (STAR Collaboration), Phys. Rev. C 73 (2006) 064907.
[2] J. Adams. *et al.* (STAR Collaboration), Phys. Rev. Lett. 95 (2005) 152301.
[3] A. Adare. *et al.* (PHENIX Collaboration), Phys. Rev. C 78 (2008) 014901.
[4] B. I. Abelev. *et al.* (STAR Collaboration), Phys. Rev. C 80 (2009) 064912.
[5] B. Alver. *et al.* (PHOBOS Collaboration), Phys. Rev. Lett. 104 (2010) 062301.
[6] B. Alver. *et al.* (PHOBOS Collaboration), Phys. Rev. C 81 (2010) 034915.
[7] S. Chatrchyan. *et al.* (CMS Collaboration), Eur. Phys. J. C 72 (2012) 10052.
[8] V. Khachatryan. *et al.* (CMS Collaboration), JHEP 1009 (2010) 091.
[9] S. Chatrchyan. *et al.* (CMS Collaboration), Phys. Lett. B 718 (2013) 795.
[10] B. Adelev. *et al.* (ALICE Collaboration), Phys. Lett. B 719 (2013) 29.
[11] A. Adare. *et al.* (PHENIX Collaboration), arXiv:1303.1794 [nucl-ex].
[12] B. Adelev. *et al.* (ALICE Collaboration), Phys. Lett. B 726 (2013) 104.
[13] S. Chatrchyan. *et al.* (CMS Collaboration), Phys. Lett. B 724 (2013) 213.
[14] I. M. Dremin, V. T. Kim, Pisma Zh. Eksp. Teor. Fiz. 92 (2010) 720.
[15] K. Werner, I. Karpenko, T. Pierog, Phys. Rev. Lett. 106 (2011) 122004.
[16] L. Cunqueiro, J. Dias de Deus, C. Pajares, Eur. Phys. J. C 65 (2010) 423.
[17] I. O. Cherednikov, N. G. Stefanis, Int. J. Mod. Phys. A 27 (2013) 1250008.
[18] S. Gavin, L. McLerran, G. Moschelli, Phys. Rev. C 79 (2009) 051902.
[19] A. Dumitru, K. Dusling, F. Gelis, J. Jalilian-Marian, T. Lappi, R. Venugopalan, Phys. Lett. B 697 (2011) 21.
[20] A. Kovner, M. Lublinsky, Phys. Rev. D 83 (2011) 034017.
[21] S. Gavin, G. Moschelli, Phys. Rev. C 85 (2012) 014905.
[22] K. Dusling, R. Venugopalan, Phys. Rev. D 87 (2013) 054014.
[23] K. Dusling, R. Venugopalan, Phys. Rev. D 87 (2013) 094034.
[24] A. Bzdak, B. Schenke, P. Tribedy, R. Venugopalan, Phys. Rev. C 87 (2013) 064906.
[25] Y. V. Kovchegov, D. E. Wertepny, arXiv:1310.6701 [hep-ph].
[26] J. Dias de Deus, C. Pajares, Phys. Lett. B 695 (2011) 211.
[27] A. Kovner, M. Lublisnky, Int. J. of Mod. Phys. E 22 (2013) 1330001.
[28] G. Agakishiev. *et al.* (STAR Collaboration), Phys. Rev. C 86 (2012) 064902.
[29] N. Armesto, M. A. Braun, E. G. Ferreiro, C. Pajares, Phys. Rev. Lett. 77 (1996) 3736.
[30] A. Rodrigues, R. Ugoccioni, J. Dias de Deus, Phys. Lett. B 458 (1999) 402.
[31] M. A. Braun, C. Pajares, Eur. Phys. J. C 16 (2000) 349.
[32] J. Dias de Deus, E. G. Ferreiro, C. Pajares, R. Ugoccioni, Eur. Phys. J. C 40 (2005) 229.
[33] A. Capella, U. P. Sukhatme, C. I. Tan, J. Tran Thanh Van, Phys. Rep. 236 (1994) 225.
[34] A. Capella, C. Pajares, A. V. Ramallo, Nucl. Phys. B 241 (1984) 75.
[35] A. B. Kaidalov, K. A. Ter-Martirosyan, Phys. Lett. B 117 (1982) 247.
[36] K. Werner, Phys. Rep. 232 (1992) 87.
[37] K. Werner, T. Hirano, I. Karpenko, T. Pierog, S. Porteboeuf, M. Bleicher, S. Haussler, Nucl. Phys. B Proc. Suppl. 196 (2009) 36.
[38] G. N. Fowler, E. M. Friedlander, R. M. Weiner, G. Wilk, Phys. Rev. Lett. 56 (1986) 14.
[39] I. Bautista, J. G. Milhano, C. Pajares, J. Dias de Deus, Phys. Lett. B 715 (2012) 230.
[40] I. Bautista, C. Pajares, J. G. Milhano, J. Dias de Deus, Phys. Rev. C 86 (2012) 034909.
[41] R. L. Ray, M. Daugherty, J. Phys. G 35 (2008) 125106.
[42] I. Bautista, L. Cunqueiro, J. Dias de Deus, C. Pajares, J. Phys. G 37 (2010) 015103.
[43] I. Bautista, J. Dias de Deus, C. Pajares, Phys. Lett. B 693 (2010) 362.
[44] I. Bautista, J. Dias de Deus, C. Pajares, Eur. Phys. J. C 72 (2012) 2038.
[45] M. A. Braun, C. Pajares, Eur. Phys. J. C 71 (2011) 1558.
[46] M. A. Braun, C. Pajares, V. V. Vechernin, Nucl. Phys. A 906 (2013) 14.